

Article

Optimization of Hybrid Ultrasonic Frequency Pulsed VP-GTAW Process Parameters on Tensile Properties of AA 5456 Alloy

Yipeng Wang ^{1,2}, Bojin Qi ^{1,2}, Baoqiang Cong ^{1,2,*} and Mingxuan Yang ^{1,2}

¹ Department of Materials Processing, Beijing University of Aeronautics and Astronautics, Beijing 100191, China; wyp092@buaa.edu.cn (Y.W.); qbj@buaa.edu.cn (B.Q.); yangmingxuan@buaa.edu.cn (M.Y.)

² MIIT Key Laboratory of Aeronautics Intelligent Manufacturing, Beijing 100191, China

* Correspondence: cong bq@buaa.edu.cn; Tel.: +86-10-8233-9961

Academic Editors: Hai-Lung Tsai and Junling Hu

Received: 17 March 2017; Accepted: 5 May 2017; Published: 8 May 2017

Abstract: Tensile properties optimization of AA 5456 aluminum alloy was carried out with hybrid ultrasonic frequency pulsed variable polarity gas tungsten arc welding (HPVP-GTAW). An orthogonal method was employed to conduct the experiments, and the tensile properties of AA 5456 aluminum alloy welded joints were measured and analyzed. Regression models were developed based on the least square estimation by taking tensile strength, yield strength, percent elongation, and ratio of reduction in area as response functions of variable polarity frequency f_L , pulse frequency f_H and a dimensionless parameter ψ , which were calculated by background current I_b , peak current I_p , and pulse duration δ , respectively. The developed regression equations were checked for validity by coefficient of correlation r^2 and confirmatory experiments. Optimum parameters of HPVP-GTAW were achieved through the discussion on response surfaces and contour plots drawn using the regression equations.

Keywords: ultrasonic frequency pulsed current; VP-GTAW; aluminum alloy; tensile properties

1. Introduction

Aluminum-magnesium alloys, which are classified as non-heat treatable and strain hardening alloy series, are extensively used in aeronautics and astronautics industries due to their great corrosion resistance, excellent fatigue properties, and fracture toughness, in addition to the general characteristics of aluminum alloys [1]. Welding fabrication is one of the key manufacturing methods for aluminum alloy parts [2]. In general, the variable polarity gas tungsten arc welding (VP-GTAW) process is popularly employed in the welding of thin aluminum alloy plates, in which the surface oxide film can be effectively cleaned by cathode atomization in the negative polarity stage and the base metal is principally melted in positive polarity stage [3].

The strengthening mechanism of non-heat treatable Al-Mg alloys, typical 5xxx series, is mainly the result of the existence of alloying elements such as magnesium and silicon that play an important role in precipitation strengthening and solid solution strengthening. Al-Mg 5xxx series contain more than 3.0% magnesium, while the vaporization of alloying elements will occur during welding fabrication. This vaporization loss may reduce the mechanical properties of welded joints by affecting the chemical compositions of molten pool [4–6]. In order to enhance the weld quality of Al-Mg alloys, metallurgical advantages of welds produced by high-frequency pulsed and magnetic arc oscillation methods are frequently investigated, including stirring effect on molten pool, refinement of grains, reduction of distortion, and control of segregation [7–9]. A novel hybrid ultrasonic frequency pulsed VP-GTAW (HPVP-GTAW) technique has been developed in which ultrasonic frequency pulsed current

is accurately superimposed in the positive polarity stage during VP-GTAW process. This process has been employed in aluminum alloy welding, and series experimental results have proven that ultrasonic frequency pulsed current is beneficial to the elimination of the weld porosity [10], the reduction of the width of HAZ [11], the increase of the weld penetration [12], the refinement of the microstructure in weld zone [13–15], and the improvement of the mechanical properties of welded joints [16–18]. However, research work on the optimization of process parameters with HPVP-GTAW has not been done before.

The purpose of the present study was to optimize the HPVP-GTAW process parameters for enhancing the mechanical properties of 5xxx aluminum alloy welded joints. Orthogonal design, a multi-factor and multi-level experimental method, was employed in this study. Using this method, some representative points were selected to design the experiments for the optimization of indicators, thereby reducing the number of experiments [19,20]. Regression analysis method was also employed by regarding tensile strength, yield strength, percent elongation, and ratio reduction in area as indicators, and regression equations were obtained using the least square estimation. The optimum parameters of HPVP-GTAW process for AA 5456 aluminum alloy were obtained by analyzing the response surfaces and contour plots based on the regression equations.

2. Experimental Procedure

2.1. Materials

The base metal used in this study was AA 5456 aluminum alloy plates with a chemical composition of Mg 5.8, Si 0.4, Mn 0.6, Zn 0.2, Cu 0.1, and Al balance (all in wt %). The gauge dimension was 200 mm × 100 mm × 3 mm. The filler material selected was 2.4 mm in diameter ER5356, with a chemical composition of Mg 5.0, Si 0.25, Mn 0.12, Zn 0.1, Cu 0.1, and Al balance (all in wt %). Typical “I” butt joints of 200 mm in length were produced by hybrid ultrasonic frequency pulsed VP-GTAW process.

2.2. Welding Process Parameters

The schematic diagram of circuit topology and the actual welding current waveform of HPVP-GTAW are shown in Figure 1. The HPVP-GTAW power source mainly includes constant current generating circuit, high frequency pulsed current generating circuit (5 KHz–40 kHz high frequency pulsed current) and full-bridge inverter circuit (0.1 KHz–1 kHz variable polarity current).

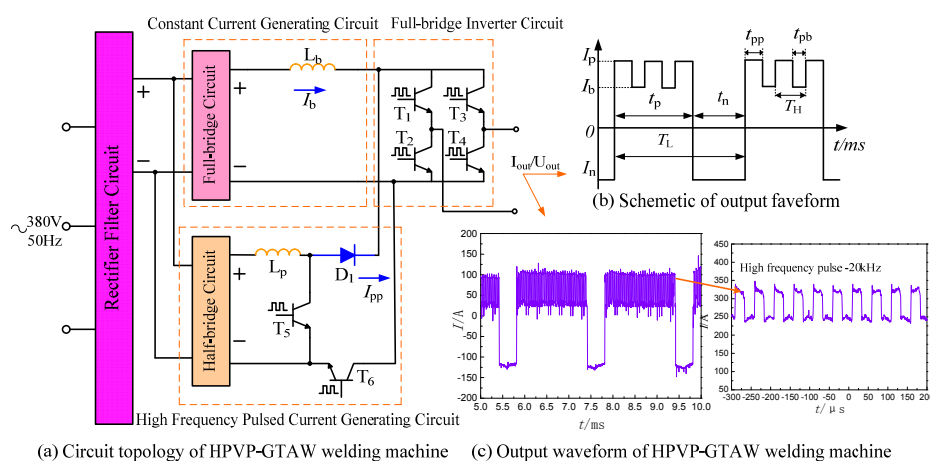


Figure 1. Schematic diagram of circuit topology and output waveform of hybrid ultrasonic frequency pulsed variable polarity gas tungsten arc welding (HPVP-GTAW). T_L —period of variable polarity current; $f_L = 1/T_L$ —variable polarity frequency; I_n —negative current; I_b —high-frequency pulsed background current; I_p —high-frequency pulsed peak current; T_H —period of pulsed current; $\delta = t_{pp}/T_H$ —pulse duration; $f_H = 1/T_H$ —pulse frequency.

According to the literature [11–13] and previous research work [14–18], among all the parameters, the characteristic parameters, such as variable polarity frequency f_L , high-frequency pulsed background current I_b , high-frequency pulsed peak current I_p , pulse duration δ and pulse frequency f_H , have a greater influence on the weld penetration and tensile properties of aluminum alloy welded joints. Then, the above-mentioned factors were taken as welding process parameters.

2.3. Variation Range of Welding Process Parameters

In order to ensure the uniformity of the input power, it is necessary to simultaneously adjust I_p , I_b and δ . G.E. Cook [21,22] stated that the average input power by pulsed current is principally determined by Equation (1).

$$P_{in} = A_1 I_{eff} + A_2 I_{avg} + A_3 \tag{1}$$

where P_{in} is the input power; I_{eff} is the effective current; I_{avg} is the average current; and A_1 , A_2 , A_3 are the constant values depending on arc length, dimension of electron, type of base metal material, and shielding gas, etc. In this research, the error range of I_{eff} and I_{avg} should be controlled within ± 5 A. Meanwhile, a dimensionless parameter ψ was introduced to represent I_p , I_b , and δ synchronously. ψ is calculated as,

$$\psi = \frac{I_p \times \delta}{I_b \times (1 - \delta)} \tag{2}$$

A large number of trials have been conducted by changing the above pulsed current parameters to obtain excellent bead appearance and full penetration. The selected working range of f_L , f_H and ψ are listed in Table 1. Other constant welding process parameters are shown in Table 2.

Table 1. Levels of welding process parameters.

Level	Factor	A: f_L /kHz	B: f_H /kHz	C: ψ
1		0.1	5	0.60 ($I_b = 75$ A, $I_p = 180$ A, $\delta = 0.2$)
2		0.5	20	2.17 ($I_b = 60$ A, $I_p = 130$ A, $\delta = 0.5$)
3		1	40	7.33 ($I_b = 60$ A, $I_p = 110$ A, $\delta = 0.8$)

Table 2. Constant welding process parameters.

Parameter	Symbol	Value	Unit
Filter wire	-	ER5356 $\phi 2.4$ mm	-
Electrode	-	WC20 $\phi 3.0$ mm	-
Argon flow rate	v_g	15	L·min ⁻¹
Welding velocity	v_w	150	mm·min ⁻¹
Feeding velocity	v_f	150	mm·min ⁻¹
Arc length	h	3	mm
Duration ratio	$t_p:t_n$	8:2	-
Negative polarity current	I_n	120	A

2.4. Selection of Orthogonal Array

In this study, there were three welding parameters, and each parameter possessed three levels. Therefore, $L_9(3^4)$ orthogonal experimental array was employed, as shown in Table 3.

Table 3. L9(3⁴) orthogonal experimental array.

No.	Factor	A: f_L /kHz	B: f_H /kHz	C: ψ	Null
1		1 (0.1)	1 (5)	1 (0.6)	1
2		1 (0.1)	2 (20)	2 (2.17)	2
3		1 (0.1)	3 (40)	3 (7.33)	3
4		2 (0.5)	1 (5)	2 (2.17)	3
5		2 (0.5)	2 (20)	3 (7.33)	1
6		2 (0.5)	3 (40)	1 (0.6)	2
7		3 (1)	1 (5)	3 (7.33)	2
8		3 (1)	2 (20)	1 (0.6)	3
9		3 (1)	3 (40)	2 (2.17)	1

2.5. Tensile Property Test

The specimens for tensile testing were cut transverse to the welding direction, and the cutting sections were selected in the middle of the welding bead as seen in Figure 2a. To ensure accuracy and repeatability, four tensile specimens were prepared for each experimental condition to calculate the average value. As shown in Figure 2b, the dimensions of the specimens were processed according to standard metallographic procedures. Tensile testing was conducted using a computer-controlled DWD-50E electronic universal tensile testing machine at a strain rate of 3 mm/min.

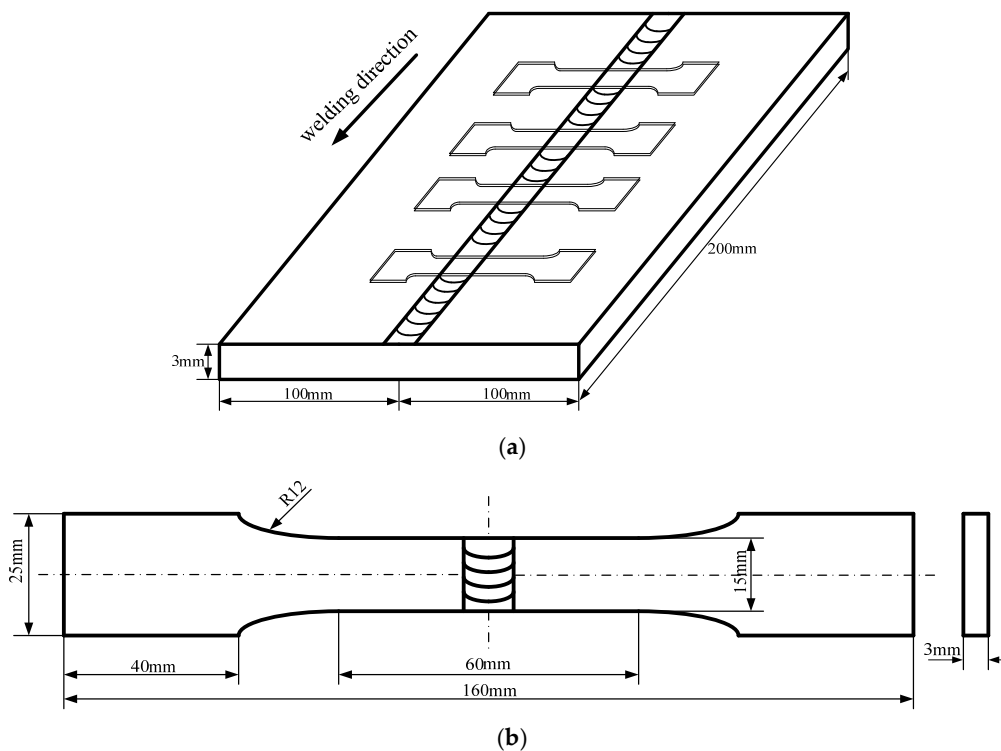


Figure 2. Dimensions of tensile specimens: (a) Schematic diagram of welding regarding to rolling direction and extraction of tensile specimens; (b) Dimensions of flat smooth tensile specimen.

The results of nine groups of orthogonal experiments are listed in the Table 4, where *TS* is the tensile strength, *YS* is the yield strength, *PE* is the percent elongation, and *RA* is the ratio of reduction in area.

Table 4. Tensile properties of AA 5456 Al alloy welded joints by orthogonal experiment.

No.	Factor	A: f_L /kHz	B: f_H /kHz	C: ψ	TS/MPa	YS/MPa	PE/%	RA/%
1		1 (0.1)	1 (5)	1 (0.6)	311	198	7.7	8.4
2		1 (0.1)	2 (20)	2 (2.17)	335	211	7.7	8.6
3		1 (0.1)	3 (40)	3 (7.33)	318	204	8.1	8.6
4		2 (0.5)	1 (5)	2 (2.17)	339	213	7.6	10.9
5		2 (0.5)	2 (20)	3 (7.33)	340	215	7.7	9.5
6		2 (0.5)	3 (40)	1 (0.6)	334	210	7.5	9.6
7		3 (1)	1 (5)	3 (7.33)	356	226	8.4	9.9
8		3 (1)	2 (20)	1 (0.6)	358	229	9.7	12.8
9		3 (1)	3 (40)	2 (2.17)	334	213	7.6	8.9

3. Regression Analysis

3.1. Development of the Regression Models

Take indicators including tensile strength, yield strength, percent elongation and ratio of reduction in area as response function of f_L, f_H and ψ . The response function can be expressed as the following:

$$y = f(f_L, f_H, \psi) \tag{3}$$

where f_L, f_H, ψ are independent variables and y is dependent variable. The function f can be developed through regression analysis. The selected regression model involves the above three factors and the interaction of high frequency parameters f_H and ψ . It can be expressed as,

$$y = \beta_0 + \beta_1(f_L) + \beta_2(f_H) + \beta_3(\psi) + \beta_4(f_L^2) + \beta_5(f_H^2) + \beta_6(\psi^2) + \beta_7(\psi f_H) \tag{4}$$

where β_0 is the regression constant; $\beta_1, \beta_2, \dots, \beta_7$ are the regression coefficients. $\beta_0, \beta_1, \beta_2, \dots, \beta_7$ are unknown parameters to be determined.

3.2. Determination of the Regression Coefficients

In order to determine the regression coefficients, the least square method is used based on the thought that the regression coefficients can be estimated when the error sum of squares Q is at its minimum, which can be expressed as Equations (5) and (6).

$$Q(\beta_0, \beta_1, \dots, \beta_p) = \sum_{i=1}^n (y_i - \beta_0 - \beta_1 x_{i1}, \dots, \beta_p x_{ip})^2 \tag{5}$$

$$Q(\hat{\beta}_0, \hat{\beta}_1, \dots, \hat{\beta}_p) = \min\{Q(\beta_0, \beta_1, \dots, \beta_p)\} \tag{6}$$

where $\hat{\beta}_0, \hat{\beta}_1, \dots, \hat{\beta}_p$ are the estimated values of the regression coefficients; n is the number of the experiments; p is the number of independent variables. The regression coefficients can be acquired when the partial differential of Q to β equals to zero, as given by Equation (7).

$$\frac{\partial Q(\beta)}{\partial \beta} = 0 \tag{7}$$

The regression coefficients are obtained through the computer-aided calculation software, and the developed regression equations are given by Equations (8)–(11).

$$TS = 304.988 + 37.9527f_L + 1.8339f_H + 2.9213\psi - 11.2392f_L^2 - 0.0395f_H^2 - 0.1002\psi^2 - 0.073\psi f_H \tag{8}$$

$$YS = 195.7674 + 17.3403f_L + 1.0875f_H + 0.2276\psi + 1.3576f_L^2 - 0.0248f_H^2 + 0.0768\psi^2 - 0.0203\psi f_H \tag{9}$$

$$PE = 8.3494 - 0.8327f_L + 0.0518f_H - 0.7894\psi + 1.9906f_L^2 - 0.0018f_H^2 + 0.0756\psi^2 + 0.0072\psi f_H \quad (10)$$

$$RA = 8.7995 + 8.7482f_L + 0.0534f_H - 1.0729\psi - 4.7774f_L^2 - 0.0029f_H^2 + 0.0719\psi^2 + 0.0168\psi f_H \quad (11)$$

3.3. Checking the Adequacy of the Regression Equations

It is necessary to examine the fitting degree between the regression equations and experimental values since the regression equations can be developed by least square method even though the experimental values are of unordered points. The adequacy of regression equation is evaluated by coefficient of correlation r^2 , which reflects the fitting degree of the regression equation and can be calculated using the following expression [4].

$$r^2 = \frac{\sum (Y_p - Y_{avg})^2}{\sum (Y_e - Y_{avg})^2} \quad (12)$$

where Y_p is the predicted value; Y_{avg} is the average value of experimental value; Y_e is the experimental value. The value of r^2 ranges from 0 to 1. When r^2 tends to 0, it means that the fitting degree of regression model is the lowest, and the fitting degree increases with the increase of r^2 . The experimental values fall on the curve drawn by regression model when r^2 approaches to 1, revealing that the regression equation perfectly fit the actual values. The coefficients of correlation corresponding to each regression equation are 0.87, 0.88, 0.84 and 0.86, respectively. It is evident that, all the coefficients of correlation r^2 of the developed models tend to 1, so that the developed regression equations are significant.

3.4. Identification of the Validity of the Regression Equations

Confirmatory experiments have been conducted to identify the validity of the developed regression equations by comparing the experimental results with the predicted values. The results are listed in Table 5, where percent deviation is calculated by,

$$\text{Percent Deviation} = \frac{EV - PV}{EV} \times 100\% \quad (13)$$

where EV is the experimental value; PV is the predicted value. From the results, it can be found that the predicted values by regression equations fit the experimental results within a reasonable error. Therefore, the regression equations can be used to predict the response of tensile properties to $f_L, f_H,$ and ψ .

Table 5. Validation of regression models by HPVP-GTAW for AA 5456 aluminum alloy.

Num.	f_L /kHz	f_H /kHz	ψ	EV	PV	Percent Deviation
Tensile strength						
1	0.2	10	0.98	324	327.7	1.2
2	0.2	30	0.98	343	331.4	3.3
3	0.7	10	4.2	330	332	0.6
4	0.7	30	4.2	341	331	2.9
Yield strength						
1	0.2	10	0.98	213	215.6	1.3
2	0.2	30	0.98	223	232.7	4.2
3	0.7	10	4.2	219	226.3	3.2
4	0.7	30	4.2	240	242.1	0.9

Table 5. Cont.

Num.	f_L /kHz	f_H /kHz	ψ	EV	PV	Percent Deviation
Percent elongation						
1	0.2	10	0.98	7.7	8.0	3.9
2	0.2	30	0.98	7.9	7.7	2.5
3	0.7	10	4.2	7.6	7.4	2.6
4	0.7	30	4.2	8.0	7.6	5.0
Ratio of reduction in area						
1	0.2	10	0.98	9.6	9.8	2.0
2	0.2	30	0.98	9.4	8.9	5.3
3	0.7	10	4.2	10.4	10.3	0.9
4	0.7	30	4.2	10.8	10.5	2.7

4. Results and Discussion

The response surfaces of tensile strength versus f_L , f_H , and ψ obtained by Equation (8) are shown in Figure 3. Tensile strength increases significantly as f_L changes from 0.1 kHz to 1 kHz in all conditions of f_H and ψ . It reaches the maximum level when f_L is 1 kHz. Therefore, 1 kHz is the optimum parameter of f_L in terms of the tensile strength. In order to determine the optimum parameters of f_H and ψ , contour plot and interaction of f_H and ψ when f_L is 1 kHz are illustrated in Figure 4. It can be found that the tensile strength monotonically rises when f_H is less than 20 kHz, where it comes to the maximum level. The tensile strength declines as f_H varies from the range of 20 kHz to 40 kHz. Therefore, 20 kHz is the optimum parameter of f_H . In the point of ψ , tensile strength increases with an increasing ψ in the condition that f_H is constant at 20 kHz. Thus, 7.33 is the optimum parameter of ψ . As shown in Figures 5 and 6, the changing tendency of yield strength is almost the same as that of tensile strength, so that they share the same optimum parameters. In summary, the optimum parameters on both tensile strength and yield strength are $f_L = 1$ kHz, $f_H = 20$ kHz and $\psi = 7.33$ (i.e., I_b is 60 A, I_p is 110 A and δ is 0.8).

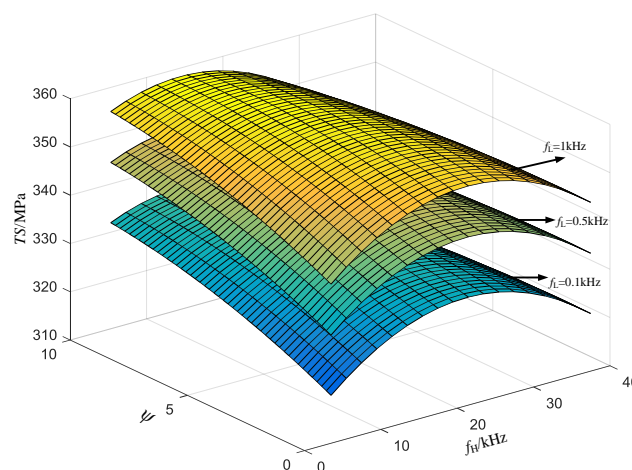


Figure 3. Response surface on tensile strength (TS).

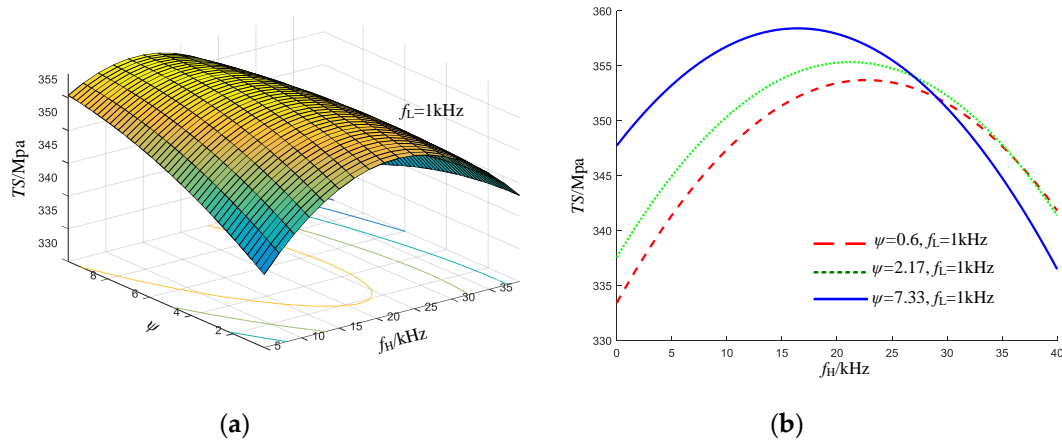


Figure 4. Contour plot of surface on tensile strength (TS): (a) contour plot of surface that f_L is 1 kHz; (b) interaction of f_H and ψ .

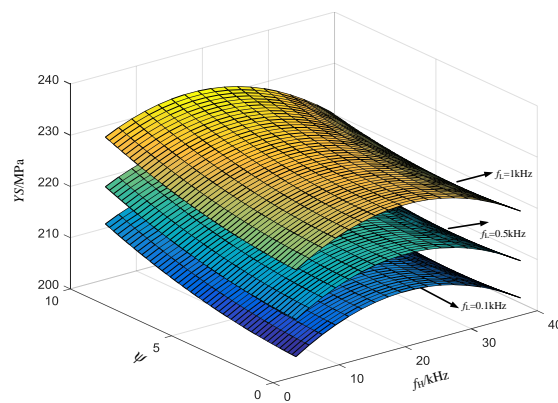


Figure 5. Response surface on yield strength (YS).

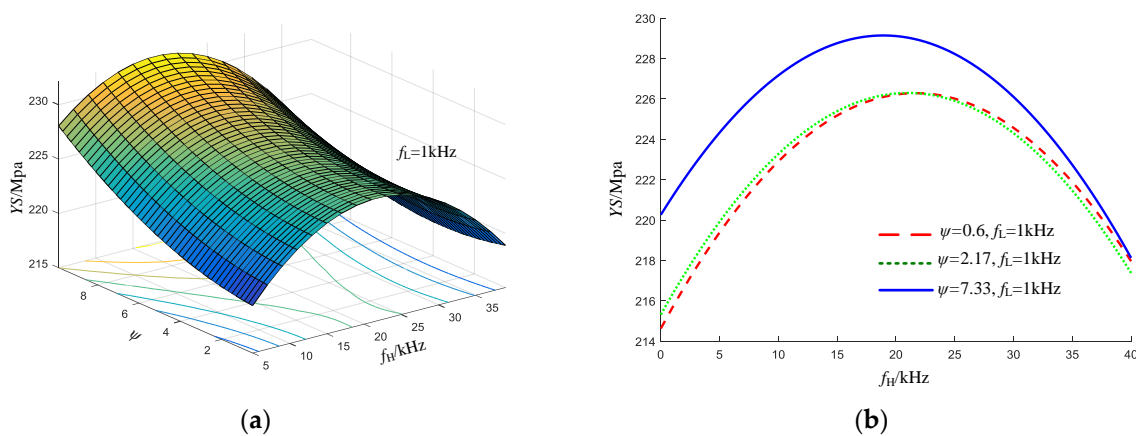


Figure 6. Contour plot of surface on yield strength (YS): (a) contour plot of surface that f_L is 1 kHz; (b) interaction of f_H and ψ .

The response surfaces and contour plots of percent elongation and ratio of reduction in area are presented in Figures 7–10, respectively. It is observed that f_L and f_H regarding to both the percent elongation and the ratio of reduction in area own the same changing tendency as tensile strength. As a consequence, 1 kHz and 20 kHz are the optimum parameters of f_L and f_H , respectively. However, as shown in Figures 8 and 10, the response of percent elongation and the ratio of reduction in area versus

ψ show completely different changing tendency. The response values are at the maximum when ψ is 0.6 under the condition that f_L is 1 kHz and f_H is 20 kHz. As a result, the optimum parameter of ψ is 0.6. In general, the optimum parameters on both percent elongation and the ratio reduction in area are $f_L = 1$ kHz, $f_H = 20$ kHz and $\psi = 0.6$ (i.e., I_b is 75 A, I_p is 180 A and δ is 0.2).

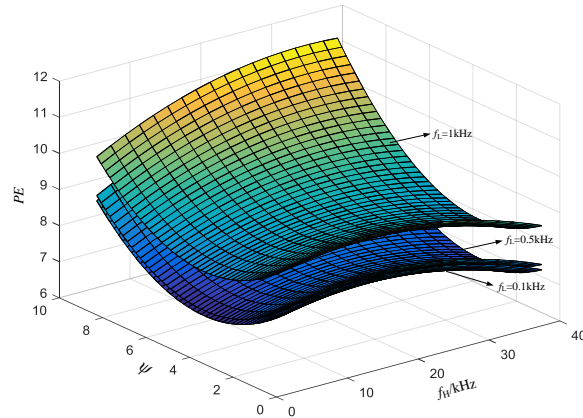


Figure 7. Response surface on percent elongation (PE).

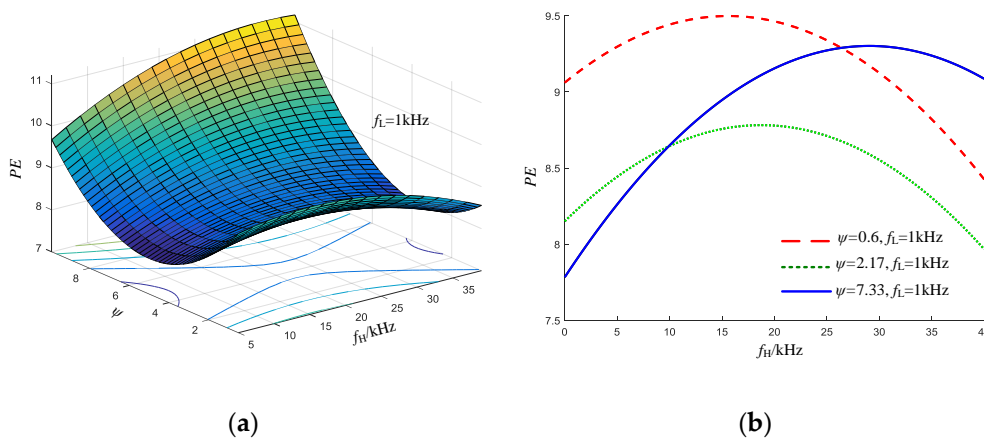


Figure 8. Contour plot of surface on percent elongation (PE): (a) contour plot of surface that f_L is 1 kHz; (b) interaction of f_H and ψ .

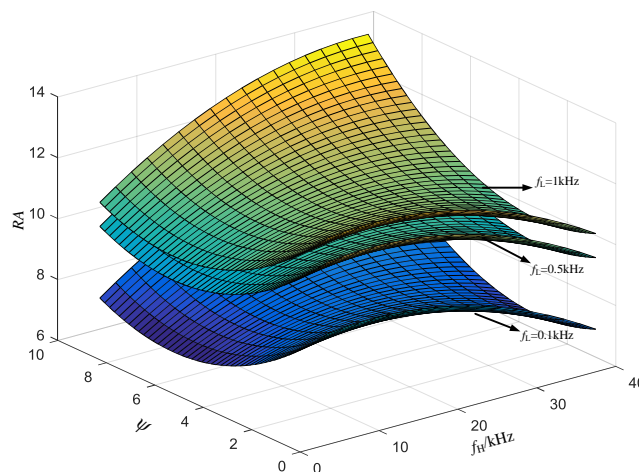


Figure 9. Response surface on ratio of reduction in area (RA).

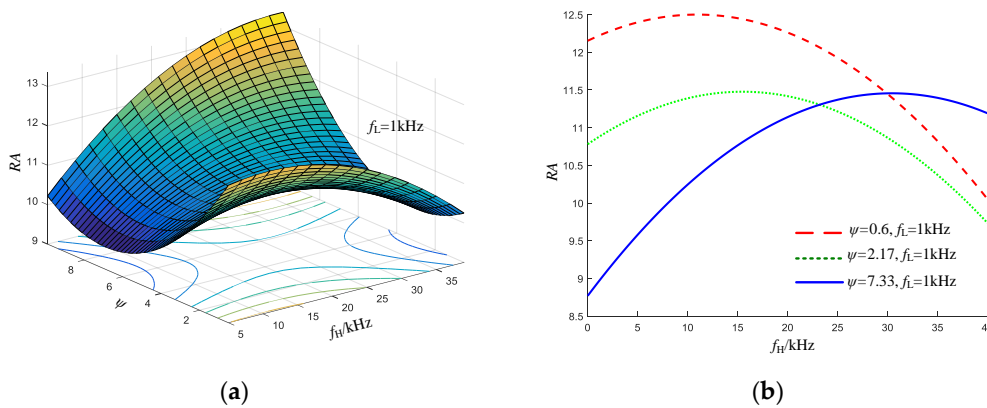


Figure 10. Contour plot of surface on ratio of reduction in area (RA): (a) contour plot of surface that f_L is 1 kHz; (b) interaction of f_H and ψ .

The optimum parameter of ψ to tensile strength and yield strength is 7.33, while that to percent elongation and ratio of reduction in area is 0.6. With every factor considered comprehensively, it can be concluded that plastic properties, including percent elongation and ratio of reduction in area, play a more important role in tensile properties than tensile strength because all the values of tensile strength in these experiments are more than 300 MPa, which is high enough in most applications. Plastic properties restrict the further improvement of mechanical properties of AA 5456 aluminum alloy [4]. Therefore, take 0.6 as the optimal parameter of ψ when plastic properties are at maximum. In conclusion, the optimum parameters, which take tensile properties into comprehensive consideration, are $f_L = 1\text{ kHz}$, $f_H = 20\text{ kHz}$ and $\psi = 0.6$ (i.e., I_b is 75 A, I_p is 180 A and δ is 0.2).

The optimum parameters obtained above happen to be Group 8 in the orthogonal experiment, in which the tensile strength is 358 MPa, the yield strength is 229 MPa, the percent elongation is 9.7%, and the ratio of reduction in area is 12.8%. Compared with the results of other experiments, the tensile properties of Group 8 are all at the maximum. The microstructure of weld zone with energy dispersive spectrometer (EDS) analysis and X ray diffraction (XRD) analysis are shown in Figures 11 and 12, respectively. The results of XRD analysis and EDS analysis show that the second-phase particles are identified as intermetallic compound Mg_2Al_3 . Weld zone of AA 5456 alloy is mainly composed of α (Al) solid solution, around which are uniformly dispersed by β (Mg_2Al_3) second-phase particles. The β (Mg_2Al_3) phase can improve the mechanical properties of AA 5456 alloy through distorting the crystal lattice around α (Al), and then prevent the dislocation motion [23]. Figure 13 reveals that the tensile fracture is characteristic of typical ductile feature due to the fact that there are obvious dimple structures densely distributed in the fracture.

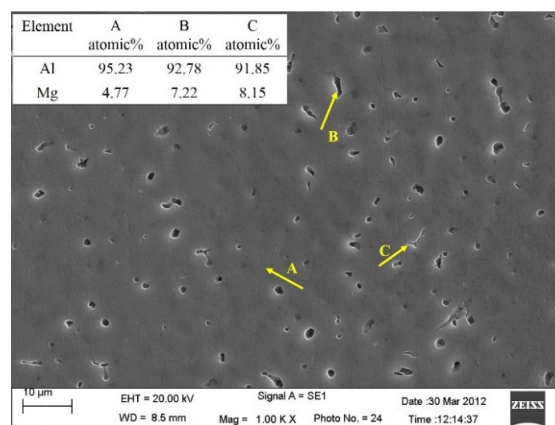


Figure 11. Microstructure of weld zone with energy dispersive spectrometer (EDS) analysis.

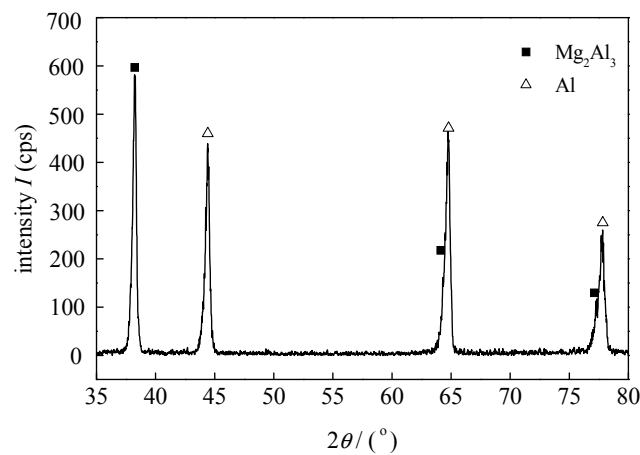


Figure 12. XRD analysis of weld zone.

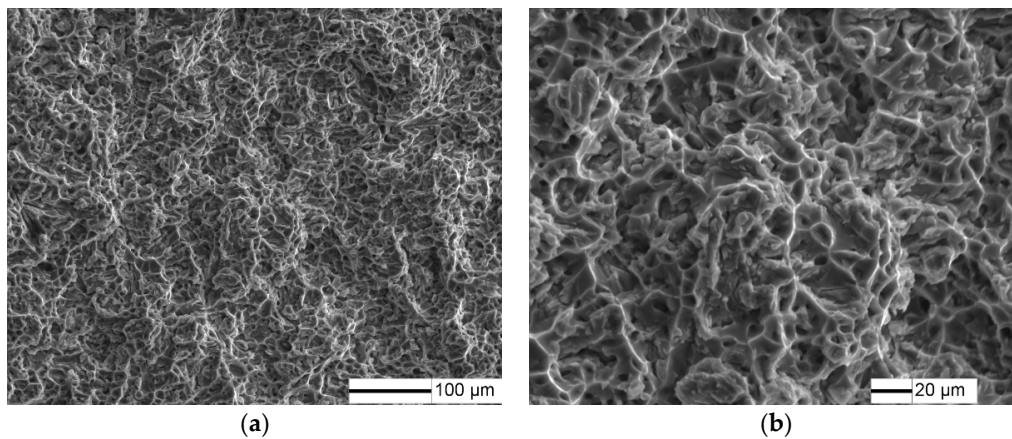


Figure 13. Tensile fracture graph (SEM) with optimum parameters: (a) $\times 200$; (b) $\times 500$.

5. Conclusions

Optimization of HPVP-GTAW process parameters, such as variable polarity frequency f_L , pulse frequency f_H , and a dimensionless factor ψ calculated by background current I_b , peak current I_p and pulse duration δ for AA 5456 aluminum alloy welded joints, have been systematically investigated. The following conclusions are drawn from the results of this study:

- (1) Regression models, which took tensile strength, yield strength, percent elongation, and ratio of reduction in area as the response functions of process parameters f_L , f_H , and ψ , were developed through least square estimation. The regression equations were proved to be effective by checking the coefficient of correlation r^2 and confirmatory experiments.
- (2) The optimum parameters of HPVP-GTAW for AA 5456 aluminum alloy were obtained by analyzing the response surfaces and the contour plots of tensile properties based on regression equations. The optimum parameters were f_L 1 kHz, f_H 20 kHz and ψ 0.6 (i.e., I_b 75 A, I_p 180 A, and δ 0.2).
- (3) The maximum tensile properties were obtained with the above optimum parameters, and the microstructural observation illustrated that there was a great deal of second-phase β (Mg_2Al_3) uniformly distributed in the weld zone, which was beneficial to the improvement of the mechanical properties of AA 5456 aluminum alloy welded joints.

Acknowledgments: The authors would like to thank all the members in Welding Manufacturing Research Group in Beihang University. The work was supported by the National Natural Science Foundation of China under Grants No. 51675031, 50975015, and 51005011.

Author Contributions: Yipeng Wang and Baoqiang Cong conceived and designed the experiments; Bojin Qi and Yipeng Wang performed the experiments; Bojin Qi and Yipeng Wang analyzed the data; Mingxuan Yang contributed analysis tools; Yipeng Wang wrote the paper.

Conflicts of Interest: The authors declare no conflict of interest.

References

1. Manti, R.; Dwivedi, D.K.; Agarwal, A. Microstructure and hardness of Al-Mg-Si weldments produced by pulse GTA welding. *Int. J. Adv. Manuf. Technol.* **2008**, *39*, 851–865. [[CrossRef](#)]
2. Elisan, D.S.M.; Ana, L.F.L.S.; Sandro, M.M.L.S. A GTA Welding Cooling Rate Analysis on Stainless Steel and Aluminum Using Inverse Problems. *Appl. Sci.* **2017**, *7*, 122. [[CrossRef](#)]
3. Pan, J.; Hu, S.; Yang, L. Investigation of molten pool behavior and weld bead formation in VP-GTAW by numerical modelling. *Mater. Des.* **2016**, *111*, 600–607. [[CrossRef](#)]
4. Kummur, A.; Sundarrajan, S. Optimization of pulsed TIG welding process parameters on mechanical properties of AA 5456 Aluminum alloy weldments. *Mater. Des.* **2009**, *30*, 1288–1297. [[CrossRef](#)]
5. Karunakaran, N.; Balasubramanian, V. Effect of pulsed current on temperature distribution, weld bead profiles and characteristics of gas tungsten arc welded aluminum alloy joints. *Trans. Nonferrous Metal. Soc. China* **2011**, *21*, 278–286. [[CrossRef](#)]
6. Giridharan, P.K.; Murugan, N. Optimization of pulsed GTA welding process parameters for the welding of AISI 304L stainless steel sheets. *Inter. J. Adv. Manuf. Technol.* **2009**, *40*, 478–489. [[CrossRef](#)]
7. Yang, M.X.; Zheng, H.; Li, L. Arc Shapes Characteristics with Ultra High Frequency Pulsed Arc Welding. *Appl. Sci.* **2017**, *7*, 45. [[CrossRef](#)]
8. Moreira, P.M.G.P.; Santos, T.; Tavares, S.M.O. Mechanical and metallurgical characterization of friction stir welding joints of AA 6061-T6 with AA6082-T6. *J. Mater. Des.* **2009**, *30*, 180–187. [[CrossRef](#)]
9. Elangovan, K.; Balasubramanian, V.; Babu, S. Predicting tensile strength of friction stir welded AA 6061 aluminium alloy joints by a mathematical model. *Mater. Des.* **2009**, *30*, 188–193. [[CrossRef](#)]
10. Yang, M.X.; Yang, Z.; Cong, B.Q. How ultrahigh frequency of pulsed gas tungsten arc welding affects weld porosity of Ti-6Al-4V alloy. *Inter. J. Adv. Manuf. Technol.* **2015**, *76*, 955–960. [[CrossRef](#)]
11. Stoekinger, G.R.; Pulsed, D.C. High frequency GTA welding of aluminum plate. *Weld. J.* **1973**, *53*, 558–567.
12. Sun, Q.J.; Lin, S.B.; Yang, C.L.; Zhao, G.Q. Penetration increase of AISI 304 using ultrasonic assisted tungsten inert gas welding. *Sci. Technol. Weld. J.* **2013**, *14*, 765–767. [[CrossRef](#)]
13. Liao, X.L.; Zhai, Q.J. Refining mechanism of the electric current pulse on the solidification structure of pure aluminum. *Acta Mater.* **2007**, *55*, 3103–3109. [[CrossRef](#)]
14. Cong, B.Q.; Qi, B.J.; Zhou, X.G. Influence of ultrasonic pulse square-wave current parameters on microstructures and mechanical properties of 2219 aluminum alloy weld joints. *Acta Metall. Sin.* **2009**, *45*, 1057–1062.
15. Cong, B.Q.; Qi, B.J.; Zhou, X.G. Microstructure and mechanical properties of hybrid pulse VPTIG arc welding of high strength aluminum alloy. *Trans. China Weld. Inst.* **2010**, *36*, 1–5.
16. Qiu, L.; Yang, C.L.; Lin, S.B. Effect of pulse current on microstructure and mechanical properties of variable polarity arc weld bead of 2219-T6 aluminum alloy. *Mater. Sci. Technol.* **2009**, *25*, 739–742. [[CrossRef](#)]
17. Zhao, J.R.; Li, Y.D. Control over arc of pulsed high frequency TIG welding and High frequency effect. *J. Tianjin Univ.* **1989**, *3*, 25–32.
18. Cook, G.E.; Eassa, E.H. The effect of high-frequency pulsing of a welding arc. *IEEE Trans. Ind. Appl.* **1985**, *1A-21*, 1294–1299. [[CrossRef](#)]
19. Ross, P.J. *Taguchi Techniques for Quality Engineering*; John Wiley & Sons: New York, NY, USA, 1997; pp. 395–476.
20. Kumar, A.; Sundarrajan, S. Selection of welding process parameters for the optimum butt joint strength of an aluminum alloy. *J. Mater. Manuf. Process.* **2006**, *21*, 779–782. [[CrossRef](#)]
21. Bingul, Z.; Cook, G.E.; Strauss, A.M. Dynamic model for electrode melting rate in gas metal arc welding process. *Sci. Technol. Weld. Join.* **2001**, *6*, 41–50. [[CrossRef](#)]

22. Nakada, M.; Shiohara, Y.; Flemings, M.C. Modification of solidification structures by pulse electric discharging. *ISIJ Int.* **1990**, *30*, 27–33. [[CrossRef](#)]
23. Yang, Z.; Qi, B.J.; Cong, B.Q. Microstructure, tensile properties of Ti-6Al-4V by ultrahigh frequency pulse GTAW with low duty cycle. *J. Mater. Proc. Technol.* **2015**, *216*, 37–47. [[CrossRef](#)]



© 2017 by the authors. Licensee MDPI, Basel, Switzerland. This article is an open access article distributed under the terms and conditions of the Creative Commons Attribution (CC BY) license (<http://creativecommons.org/licenses/by/4.0/>).